

Communication

# Enhancement of Hydrogen Adsorption on Spray-Synthesized HKUST-1 via Lithium Doping and Defect Creation

Masaru Kubo \* , Tomoki Matsumoto and Manabu Shimada 

Department of Advanced Science and Engineering, Graduate School of Advanced Science and Engineering, Hiroshima University, Kagamiyama 1-4-1, Higashi-Hiroshima 739-8527, Hiroshima, Japan; [smd@hiroshima-u.ac.jp](mailto:smd@hiroshima-u.ac.jp) (M.S.)

\* Correspondence: [mkubo@hiroshima-u.ac.jp](mailto:mkubo@hiroshima-u.ac.jp); Tel.: +81-82-424-7851

**Abstract:** We prepared HKUST-1 ( $\text{Cu}_3\text{BTC}_2$ ;  $\text{BTC}^{3-} = 1,3,5\text{-benzenetricarboxylate}$ ) using a spray synthesis method with Li doping and defect created via partial replacement of  $\text{H}_3\text{BTC}$  with isophthalic acid (IP) to enhance the  $\text{H}_2$  adsorption capacity. Li-doping was performed by incorporating  $\text{LiNO}_3$  in HKUST-1 via spray synthesis and subsequent thermal treatment for decomposing  $\text{NO}_3^-$ , which enhances  $\text{H}_2$  uptake at 77 K and 1 bar per unit mass and per unit area from 2.37 wt% and 4.16 molecules/ $\text{nm}^2$  for undoped HKUST-1 to 2.47 wt% and 4.33 molecules/ $\text{nm}^2$ , respectively. Defect creation via the replacement of the  $\text{BTC}^{3-}$  linker with the  $\text{IP}^{2-}$  linker slightly in HKUST-1 skeleton did not affect  $\text{H}_2$  uptake. Both Li-doping and defect creation significantly enhanced  $\text{H}_2$  uptake to 3.03 wt%, which was caused by the coordination of Li ions with free carboxylic groups of the created defects via IP replacement.

**Keywords:** HKUST-1; metal–organic frameworks; hydrogen adsorption; lithium doping; defect creation



**Citation:** Kubo, M.; Matsumoto, T.; Shimada, M. Enhancement of Hydrogen Adsorption on Spray-Synthesized HKUST-1 via Lithium Doping and Defect Creation. *Materials* **2023**, *16*, 5416. <https://doi.org/10.3390/ma16155416>

Academic Editors: Jatuporn Wittayakun, Kittipong Chainok and Frank Roessner

Received: 6 July 2023

Revised: 24 July 2023

Accepted: 1 August 2023

Published: 2 August 2023



**Copyright:** © 2023 by the authors. Licensee MDPI, Basel, Switzerland. This article is an open access article distributed under the terms and conditions of the Creative Commons Attribution (CC BY) license (<https://creativecommons.org/licenses/by/4.0/>).

## 1. Introduction

Global warming caused by  $\text{CO}_2$  emissions and the depletion of fossil fuels has created an urgent demand for environmentally friendly alternative energy systems [1]. Hydrogen ( $\text{H}_2$ ) is an important alternative energy source to fossil fuels. A  $\text{H}_2$ -based energy system using fuel cells is expected to be central to a sustainable, recycling-oriented society owing to its high energy efficiency, low emissions of environmentally hazardous substances such as  $\text{CO}_2$  and  $\text{NO}_x$ , and its ability to be reproduced using solar energy. However, the major challenge in realizing a  $\text{H}_2$  economy using fuel cells is its storage [2–4]. The U.S. Department of Energy requires on-board  $\text{H}_2$  storage systems of fuel-cell vehicles with 5.5 wt% or 40  $\text{kg}/\text{m}^3$  of  $\text{H}_2$  tanks by 2025 [5].

Metal–organic frameworks (MOFs), which are crystalline porous materials consisting of coordination bonds between organic linkers and metal ions/clusters, have emerged as promising materials for  $\text{H}_2$  storage, owing to their exceptionally high surface area and pore volume [6–8]. At a low temperature (77 K) and high pressure, MOFs show exceptionally good  $\text{H}_2$  uptake, for example, the NU-1103 MOF has exhibited an  $\text{H}_2$  uptake of 13.0 wt% at 77 K and 100 bar [9]. However, because of the weak interaction between the MOF wall and  $\text{H}_2$  molecules, the  $\text{H}_2$  uptake at ambient temperatures is significantly smaller (just 2.8 wt% at 295 K and 100 bar for NU-1103 [9]). To overcome this weak interaction, the impregnation of strong adsorption sites into MOFs has been suggested as a way to improve the  $\text{H}_2$  uptake.  $\text{Li}^+$  ions are promising candidates for such an application owing to their low atomic weight and high affinity for molecular  $\text{H}_2$  as a result of charge-induced dipole interactions [10,11]. Theoretical investigations into Li-doped MOFs have suggested that  $\text{H}_2$  capacities of over 4.5 wt% under ambient conditions are achievable [12,13]. While experimental work is yet to reach those levels, the results thus far have been promising. For example,  $\text{Li}^+$ -doped hydroxyl-MIL-53(Al) and MIL-53(Al) improved the  $\text{H}_2$  uptake at 77 K and 1 bar from 0.5 wt% to 1.7 wt% and from 1.66 wt% to 1.84 wt%, respectively [14,15];  $\text{Li}^+$ -exchanged

NOTT-201 and MOF-5 exhibited the enhancement of H<sub>2</sub> uptake from 0.96 wt% to 1.02 wt% and from 1.23 wt% to 1.39 wt%, respectively [16,17]; Li<sup>+</sup>-doped MIL-101 exhibited the enhancement of H<sub>2</sub> uptake from 1.54 wt% to 2.65 wt% [18]. Methods for Li<sup>+</sup> doping include the reduction of the MOF skeleton via organometallic lithium [14], Li exchange with protons of hydroxyl-modified MOFs [17,19] or anionic MOFs [16], and the thermal treatment of LiNO<sub>3</sub>-impregnated MOFs [15,18,20]. The thermal treatment of LiNO<sub>3</sub>-MOF, by which NO<sub>3</sub><sup>−</sup> anions in the LiNO<sub>3</sub>-impregnated MOF is thermal decomposed to NO and/or N<sub>2</sub>O gas at 200 °C [15], is preferred because Li doping can be achieved under moderate conditions compared with the other two methods.

Another way to enhance H<sub>2</sub> uptake is to create defects in the MOF skeletons that lack coordination bonding between linkers and metals. The exposed linker and metals act as strong adsorption sites that enhance gas adsorption (H<sub>2</sub> [21], CO [22], CO<sub>2</sub> [23], and C<sub>3</sub>H<sub>8</sub> [24]). By replacing the organic linker in the parent MOF structure with a partially fragmented linker, defects can be created without altering the MOF structure [25]. In another way, the number of defects can be changed via the synthesis procedure [26].

We recently developed a continuous spray synthesis method that forms MOF nanocrystals in a short time via evaporation of droplets of a sprayed MOF precursor solution [27,28]. Rapid MOF crystallization using this method forms many missing bonds that enhance the H<sub>2</sub> uptake [26,29]. This method also enables the preparation of nanoparticle composite MOFs by adding nanoparticles to a sprayed solution [30,31]. Similar to nanoparticle incorporation, LiNO<sub>3</sub> is also expected to be incorporated into HKUST-1 by adding it to the sprayed solution. Thus, the spray synthesis method enables both Li-doping and defect creation for the enhancement of the H<sub>2</sub> storage capacity of MOFs.

In this study, we prepared a Li-doped HKUST-1 MOF (Cu<sub>3</sub>(BTC)<sub>2</sub>; H<sub>3</sub>BTC = 1,3,5-benzenetricarboxylic acid) via thermal decomposition of NO<sub>3</sub><sup>−</sup> in LiNO<sub>3</sub>-HKUST-1, synthesized via the spray-assisted synthesis method and subsequent thermal decomposition in a vacuum. In addition, we partially substituted H<sub>3</sub>BTC with isophthalic acid (IP = 1,3-benzenedicarboxylic acid) to form more defects in the HKUST-1 skeleton (defected-HKUST-1). Furthermore, we demonstrated both Li doping and defect creation into HKUST-1 via spray synthesis. We evaluated the crystallinity using X-ray diffraction (XRD) measurements, porous characteristics using nitrogen adsorption measurements, and H<sub>2</sub> adsorption properties at 77 K.

## 2. Materials and Methods

### 2.1. Chemicals

Copper nitrate trihydrate (Cu(NO<sub>3</sub>)<sub>2</sub>·3H<sub>2</sub>O, 99%), lithium nitrate (LiNO<sub>3</sub>, 99%), 1 M HCl aqueous solution (for volumetric analysis), copper standard solution (Cu 1000), lithium standard solution (Li 1000), 20% deuterium chloride solution in D<sub>2</sub>O (DCI/D<sub>2</sub>O, 99.5%) N,N-dimethylformamide (DMF, 99%), and ethanol were purchased from Fuji-film Wako Pure Chemical Co. (Osaka, Japan), and 1,3,5-benzenetricarboxylate (H<sub>3</sub>BTC, 98%) and dimethyl sulfoxide-d<sub>6</sub> (DMSO-d<sub>6</sub>, 99% contains 1% TMS) were purchased from Sigma-Aldrich (Burlington, MA, USA). All reagents were used without further purification.

### 2.2. Preparation of Precursor Solution of Li-Doped HKUST-1 (Li-HKUST-1)

The precursor solution for Li-HKUST-1 was a mixture of 5 mL of 0.75 mM Cu(NO<sub>3</sub>)<sub>2</sub> aqueous solution and 10 mL of 0.25 mM H<sub>3</sub>BTC solution in a co-solvent containing 5 mL each of ethanol and N,N-dimethylformamide (DMF). First, 0.026–0.259 g of LiNO<sub>3</sub> was added to the Cu(NO<sub>3</sub>)<sub>2</sub> solution before mixing with the H<sub>3</sub>BTC solution. The Li/Cu ratios were 10, 20, and 200 mol%. Li-HKUST-1 samples obtained from these solutions are denoted as Li-10, Li-20, and Li-200, respectively. HKUST-1 without Li<sup>+</sup> was synthesized using the same procedure but without the addition of LiNO<sub>3</sub>.

### 2.3. Preparation of Precursor Solutions of Defect-HKUST-1 (*d*-HKUST-1) and Li-Doped Defect-HKUST-1 (*Li-d*-HKUST-1)

An amount of isophthalic acid (IP) was added to the H<sub>3</sub>BTC solution. The ratio of IP/(IP+H<sub>3</sub>BTC) in the organic linker solution was varied as 6.25, 12.5, and 25 mol%, without changing the total organic linker concentration (0.25 mM); 10 mL of the organic solution was mixed with 5 mL of a 0.75 mM Cu(NO<sub>3</sub>)<sub>2</sub> aqueous solution. The *d*-HKUST-1 samples obtained from these solutions are denoted as *d*6.25, *d*12.5, and *d*25, respectively. To prepare *Li-d*-HKUST-1, 0.026 g of LiNO<sub>3</sub> was added to an aqueous Cu(NO<sub>3</sub>)<sub>2</sub> solution at a 10 mol% of Li/Cu ratio. The *Li-d*-HKUST-1 samples obtained from these solutions are denoted as *Li-d*6.25, *Li-d*12.5, and *Li-d*25, respectively.

### 2.4. Spray Synthesis of *Li*-HKUST-1, *d*-HKUST-1, and *Li-d*-HKUST-1

*Li*-HKUST-1 and *Li-d*-HKUST-1 were synthesized using a homemade spray dryer, which consisted of a two-fluid nozzle, a spray chamber equipped with an inlet of swirling air to prevent deposition loss of droplets, a heating tube, and a filter holder [29]. The precursor solution was fed into the nozzle at a flow rate of 3 mL/min and sprayed with clean air at a flow rate of 12 L/min. Swirling air was supplied at a flow rate of 30 L/min and temperature of 180 °C. The sprayed droplets were then heated in a heating tube at 200 °C. The samples were then collected using a glass filter, washed with water and ethanol, ultrasonicated, and centrifugated to eliminate residual precursors [27]. After centrifugation, samples were dried at 60 °C for 3 h. Thermal decomposition of NO<sub>3</sub><sup>−</sup> ions was conducted at 200 °C under vacuum for 5 h.

### 2.5. Characterization

Powder XRD patterns were recorded on a Miniflex 600 instrument (Rigaku Corp., Tokyo, Japan) with Cu K $\alpha$  radiation (wavelength 1.5406 Å). Inductively coupled plasma atomic emission spectrometry (ICP-AES) (SPS3000, Seiko Instrument Inc., Chiba, Japan) measurements were conducted for the quantitative analysis of the Li and Cu species in the samples. Before the ICP-AES measurements, 10 mg of each sample was dissolved in 1 mL of 1 M HCl aqueous solution. After dissolution, deionized water was carefully added to the solution until the volume reached 10 mL. The concentrations of Li and Cu in the sample solution were confirmed via the emission intensities at 670.784 and 327.396 nm for Li and Cu, respectively. Nitrogen adsorption–desorption measurements were carried out on an automated micropore gas analyzer (AUTOSORB-1-MP, Quantachrome Instruments, Boynton Beach, FL, USA) at 77 K after sample activation at 180 °C and 0.1 Pa for 6 h. The specific surface areas of the samples were calculated from nitrogen adsorption isotherms using the Brunauer–Emmett–Teller (BET) method in the range of 0.01 <  $P/P_0$  < 0.05. The micropore volumes were calculated using the  $t$ -plot method. To determine the IP ratio in the samples, the samples were digested via sonication in a mixture of DCl/D<sub>2</sub>O (35% solution) and DMSO-d<sub>6</sub>. The <sup>1</sup>H NMR spectra were recorded on a Varian System 500 spectrometer. In the <sup>1</sup>H NMR spectra, the ratio of the dicarboxylic acids was determined by comparing the integrals for the signal at  $\delta$  = 8.64 ppm (H<sub>3</sub>BTC) with those for the signals at  $\delta$  = 8.48, 8.18, and 7.69 ppm (IP).

## 3. Results

### 3.1. *Li*-HKUST-1

*Li*-HKUST-1 was prepared by changing the Li/Cu ratio in the precursor solution to 10, 20, and 200 mol% (denoted as *Li*-10, *Li*-20, and *Li*-200, respectively). Figure 1a shows the XRD patterns of HKUST-1, *Li*-10, *Li*-20, and *Li*-200. All *Li*-HKUST-1 samples exhibit patterns attributed to HKUST-1, indicating that HKUST-1 is successfully formed even in the presence of LiNO<sub>3</sub>. The peak intensities of *Li*-10 and *Li*-20 are almost the same. However, that of *Li*-200 is slightly smaller, which indicates that the crystallinity of *Li*-200 is lower than that of *Li*-10 and *Li*-20; this is due to the excess amount of LiNO<sub>3</sub> present. LiNO<sub>3</sub> would be precipitated during droplet evaporation, which prevented the crystallization

of HKUST-1 in droplets. Our previous study on the fabrication of the nanocomposites of HKUST-1 and  $\text{Fe}_3\text{O}_4$  nanoparticles also showed that an excess amount of nanoparticles prevents crystallization [31].

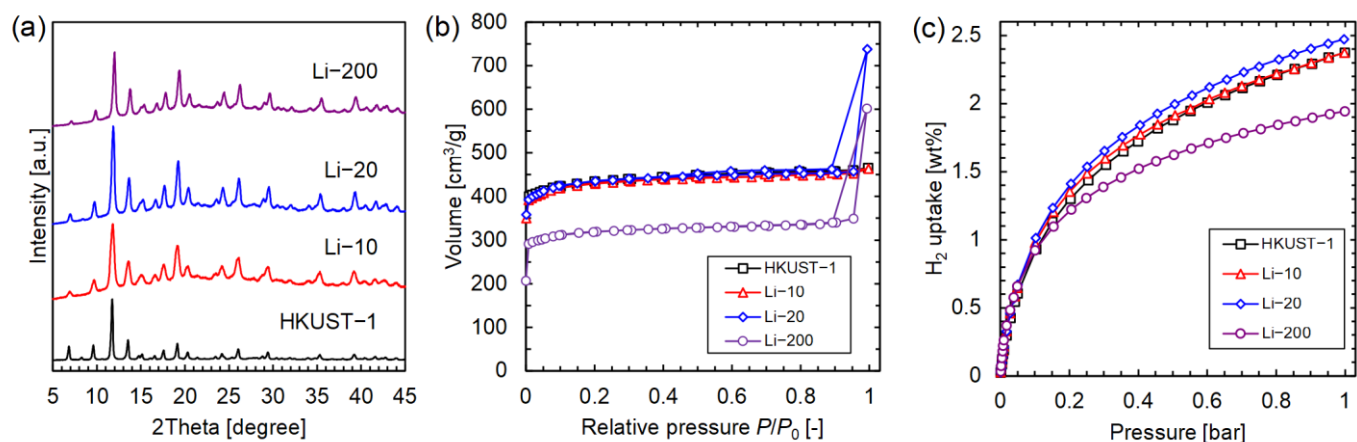


**Figure 1.** (a) XRD patterns, (b) N<sub>2</sub> adsorption isotherms, and (c) H<sub>2</sub> adsorption isotherms of HKUST-1 (black), Li-10 (red), Li-20 (blue), and Li-200 (purple).

Figure 1b shows the nitrogen adsorption isotherms of the samples. Li-10 and Li-20 show almost the same type-I isotherm as HKUST-1, whereas Li-200 shows a decrease in adsorption at all relative pressures. The BET surface areas, as summarized in Table 1, are 1705 m<sup>2</sup>/g for HKUST-1, 1548 m<sup>2</sup>/g for Li-10, 1706 m<sup>2</sup>/g for Li-20, and 1251 m<sup>2</sup>/g for Li-200. The small BET surface area of Li-200 is attributed to its low crystallinity, as revealed by the XRD pattern.

**Table 1.** Summary of the elemental analysis, and N<sub>2</sub> and H<sub>2</sub> adsorption measurements for Li-HKUST-1.

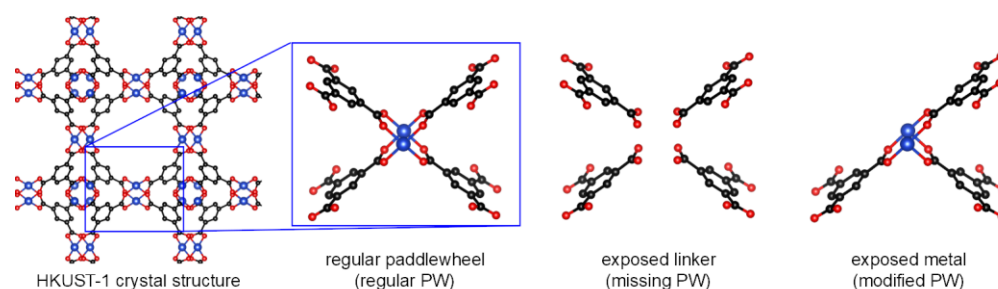
Sample	Li/Cu (mol%)	BET Surface Area (m <sup>2</sup> /g)	H <sub>2</sub> Uptake at 77 K and 1 Bar (wt%)
HKUST-1	0	1705	2.37
Li-10	0.29	1548	2.37
Li-20	0.24	1706	2.47
Li-200	0.93	1251	1.94

The Li/Cu ratios in Li-HKUST-1 were determined via elemental analysis using ICP-AES, and they were determined to be 0.29, 0.24, and 0.93 mol% in Li-10, Li-20, and Li-200, respectively, indicating the presence of Li in all three samples (Table 1). The Li/Cu ratio in Li-HKUST-1 is much lower than that in the precursor solution because of the dissolution and removal of  $\text{LiNO}_3$  by washing.

Figure 1c shows the H<sub>2</sub> adsorption isotherms of the samples at 77 K. H<sub>2</sub> uptakes of the samples are summarized in Table 1. The H<sub>2</sub> uptake of HKUST-1 is 2.37 wt% at 1 bar, which is consistent with that of our previous result [29]. Li-10 exhibits the same H<sub>2</sub> uptake as HKUST-1, even though its surface area was smaller. Li-20, the surface area of which is the same as that of HKUST-1, exhibits a higher H<sub>2</sub> uptake of 2.47 wt%. Meanwhile, Li-200 exhibits a lower H<sub>2</sub> uptake (1.95 wt%), owing to the decrease in surface area.

Previous studies on Li doping using  $\text{LiNO}_3$  suggested that Li ions were coordinated with the free carboxyl groups via solid-state NMR and XPS analyses [15,20]. Scheme 1 presents the possible defects generated via the spray synthesis method. The HKUST-1 crystal structure is constructed from paddlewheels formed via the coordination bonds of four BTC carboxyl groups and two Cu ions. Rapid crystallization during droplet evaporation would form two types of defects, which are exposed linkers and metals.

Li ions would coordinate with free carboxyl groups of the exposed linker, which would act as the additional adsorption sites for H<sub>2</sub> molecules.



**Scheme 1.** Different types of defects created via the spray synthesis method. (black, red, and blue balls represents hydrogen, oxygen, and copper atoms, respectively).

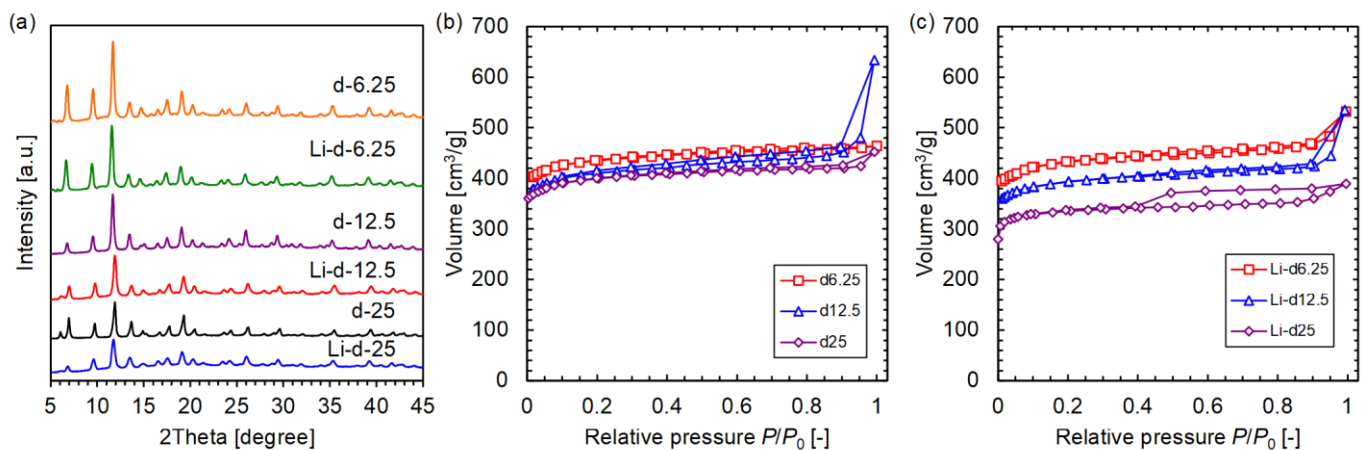
### 3.2. Li-d-HKUST-1

To intentionally introduce defects into the HKUST-1 skeleton, the organic ligand H<sub>3</sub>BTC of HKUST-1 was partially replaced with IP. Defected-HKUST-1 (d-HKUST-1) was prepared by changing the ratio of IP/(IP+H<sub>3</sub>BTC) in the organic linker solution to 6.25, 12.5, and 25 mol% (denoted as d6.25, d12.5, and d25, respectively). Li-defected-HKUST-1 (Li-d-HKUST-1) was prepared with an IP/(IP+H<sub>3</sub>BTC) ratio and Li/Cu ratio of 10 mol% (denoted as Li-d6.25, Li-d12.5, and Li-d25, respectively). Table 2 summarizes the Li/Cu ratio, IP ratio, BET surface areas, and H<sub>2</sub> uptakes at 77 K and 1 bar of the samples.

**Table 2.** Summary of elemental analysis, and N<sub>2</sub> and H<sub>2</sub> adsorption measurements for d-HKUST-1 and Li-d-HKUST-1.

Sample	Li/Cu (mol%)	IP/(BTC+IP) (%)	BET Surface Area (m <sup>2</sup> /g)	H <sub>2</sub> Uptake at 77 K and 1 Bar (wt%)
d6.25	0	4.8	1714	2.42
d12.5	0	10.3	1609	2.41
d25	0	22.2	1569	2.23
Li-d6.25	0.64	4.2	1687	2.63
Li-d12.5	0.85	10.9	1544	3.03
Li-d25	0.51	19.9	1330	2.14

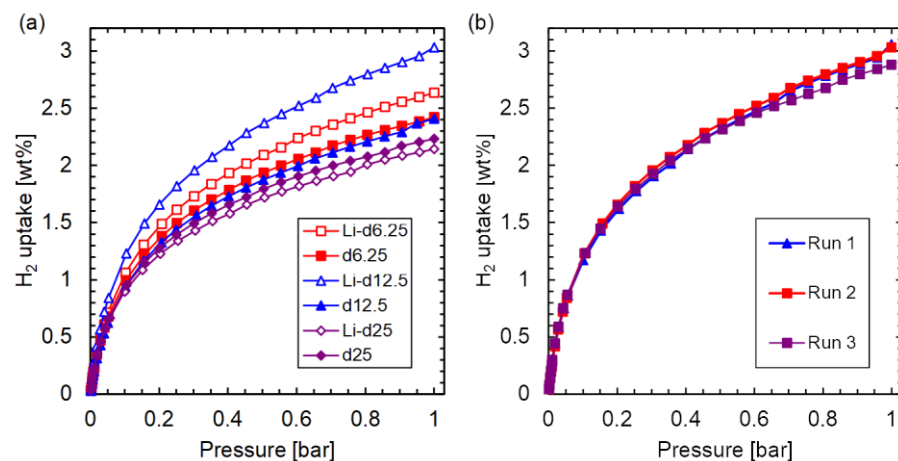
Figure 2a shows the XRD patterns of d-HKUST-1 and Li-d-HKUST-1. All samples exhibit patterns attributed to HKUST-1, indicating that the replacement of H<sub>3</sub>BTC with IP and further Li impregnation does not affect the crystallization of HKUST-1 via the spray synthesis method. The Li/Cu ratio was analyzed using ICP-AES. It was found that the Li contents in Li-d6.25, Li-d12.5, and Li-d25 are 0.64, 0.85, and 0.51 mol%, respectively; these are higher than that in the case without IP (0.29 mol% of Li-10). The ratios of IP in d-HKUST-1 and Li-d-HKUST-1 were measured via <sup>1</sup>H NMR after dissolution of the samples. The NMR spectra of d-HKUST-1 and Li-d-HKUST-1 are shown in Figures S1 and S2. The ratio of IP/(BTC+IP) calculated by integrating the signal at  $\delta = 8.64$  ppm for H<sub>3</sub>BTC with the signals at  $\delta = 8.48, 8.18,$  and  $7.69$  ppm for IP are listed in Table 2. Although the ratios are slightly lower than those in the precursor solution, IP was successfully introduced to the HKUST-1 crystal structure.



**Figure 2.** (a) XRD patterns and N<sub>2</sub> adsorption isotherms for (b) d-HKUST-1 and (c) Li-d-HKUST-1.

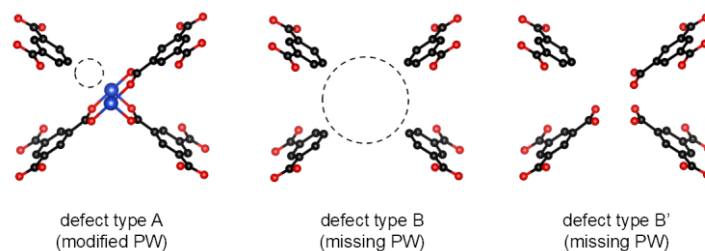
Figure 2b,c show the N<sub>2</sub> adsorption isotherms of d-HKUST-1 and Li-d-HKUST-1, respectively. The BET surface areas of d6.25 and Li-d6.25 were 1714 and 1687 m<sup>2</sup>/g, respectively, which were similar to those of HKUST-1, indicating that there was no change in pore structure owing to low IP replacement. Conversely, with increasing IP ratio, the BET surface areas decreased to 1609, 1569, 1544, and 1330 m<sup>2</sup>/g for d12.5, d25, m<sup>2</sup>/g, Li-d12.5, and Li-d25, respectively. From the literature, the defect creation via IP replacement increased with BET surface area [25,32]. However, the results of this study show a lower BET surface area, which would be due to slightly lower crystallinity. The crystallization via the spray synthesis method occurred in <1 s. Presumably, the presence of IP, the incorporation of which is considered thermodynamically unstable, hindered crystallization in the short period and reduced the BET surface area. The lower IP ratio in the sample than that in the precursor solution is also due to the low crystallinity.

Figure 3a shows the H<sub>2</sub> adsorption isotherms of d-HKUST-1 and Li-d-HKUST-1 at 77 K. The H<sub>2</sub> uptake of d-HKUST-1 reaches 2.42 wt%, which is almost consistent with that of HKUST-1. Conversely, Li-d-HKUST-1 exhibits higher H<sub>2</sub> uptake than HKUST-1 except for Li-d25. In particular, Li-d12.5 exhibits 3.03 wt% of H<sub>2</sub> uptake at 77 K and 1 bar, which is 27% higher than that of HKUST-1. To confirm whether the improved H<sub>2</sub> adsorption on Li-d12.5 is reproducible, the other two samples were prepared. Figure 3b shows the isotherms of the three samples. The H<sub>2</sub> uptakes at 1 bar were 3.03, 3.06, and 2.88 wt% with no significant difference, indicating the reproducibility of the enhancement of H<sub>2</sub> adsorption by combining Li-doping and defect creation via IP replacement.



**Figure 3.** (a) H<sub>2</sub> adsorption isotherms at 77 K of d-HKUST-1 and Li-d-HKUST-1 and (b) reproducibility test for Li-d12.5.

The enhancement of H<sub>2</sub> uptake in Li-d-HKUST-1 is discussed by considering defects. The possible defects in d-HKUST-1 and Li-d-HKUST-1 are the three additional defects shown in Scheme 2, as well as the two defects shown in Scheme 1. Defect types A and B have been proposed in the literature [22,25,32]. Using Cu(NO<sub>3</sub>)<sub>2</sub> as the copper source, type B defects are more abundant [25]. However, considering the amount of IP, it is unlikely that all four linkers were IP. There may be defects, such as type B', with exposed BTC linkers. Similar to the discussion on Li-HKUST-1, the free carboxylic groups of type B' defects coordinated with that of Li ions, which act as additional adsorption sites on H<sub>2</sub> molecules, resulting in an increase in H<sub>2</sub> uptake.



**Scheme 2.** Possible defects in d-HKUST-1. (black, red, and blue balls represents hydrogen, oxygen, and copper atoms, respectively).

Finally, we compared the results of other studies on Li doping into MOF. Table S1 summarizes the Li-doping agents, the ratio of Li to metal, BET surface area, and H<sub>2</sub> uptakes of other Li-doped MOFs. Compared with the improvements of 10–72% in H<sub>2</sub> uptake by Li-doping, an improvement of 27% for Li-d12.5 is not significantly high. However, the absolute H<sub>2</sub> uptake of Li-d12.5 is 3.03 wt% at 77 K and 1 bar, and this is higher than those of most of the Li-doped MOFs. Furthermore, the amount of Li is lower than those of other Li-doped MOFs, and therefore, there is potential for further improvements in H<sub>2</sub> uptake by increasing the Li-doping amounts.

#### 4. Conclusions

Li doping and defect creation were performed on spray-synthesized HKUST-1 to improve its H<sub>2</sub> adsorption properties. Li-doping was conducted via LiNO<sub>3</sub> incorporation and subsequent thermal decomposition of NO<sub>3</sub><sup>−</sup>. Li-HKUST-1 resulted in the enhancement of H<sub>2</sub> uptake from 2.37 wt% for the non-treated MOF to 2.47 wt%, at 77 K and 1 bar. Defect creation in HKUST-1 was conducted via partial replacement of the original linker, H<sub>3</sub>BTC, with a fragmented linker, IP, which resulted in a H<sub>2</sub> uptake up to 2.42 wt%. Combining Li-doping and defect creation significantly improved H<sub>2</sub> uptake to 3.03 wt% (27% enhancement). This research provides a facile and efficient process for the fabrication of a MOF-based H<sub>2</sub> storage material with additional adsorption sites resulting from the presence of Li cations and defects.

**Supplementary Materials:** The following supporting information can be downloaded at: <https://www.mdpi.com/article/10.3390/ma16155416/s1>, References [33–35] are cited in the supplementary materials; Figures S1 and S2: <sup>1</sup>H NMR spectra of the digested samples; Table S1: Comparison of Li doping agent, Li/metal ratio, surface area, and H<sub>2</sub> uptake at 77 K and 1 bar for other Li-doped MOFs.

**Author Contributions:** Conceptualization, M.K.; methodology, M.K. and T.M.; validation, M.K. and T.M.; investigation, M.K. and T.M.; resources, M.K. and M.S.; data curation, M.K. and T.M.; writing—original draft preparation, M.K.; writing—review and editing, M.K., T.M., and M.S.; visualization, M.K.; supervision, M.K.; project administration, M.K.; funding acquisition, M.K. and M.S. All authors have read and agreed to the published version of the manuscript.

**Funding:** This study is supported in part by the Grant-in-Aid for Young Scientists (A) no. 16H06128 and Grant-in-Aid for Scientific Research (C) no. 20K05209 and 21K04750 of the Japan Society for the Promotion of Science.

**Institutional Review Board Statement:** Not applicable.

**Informed Consent Statement:** Not applicable.

**Data Availability Statement:** Data are contained within the article.

**Conflicts of Interest:** The authors declare no conflict of interest.

## References

1. Stocker, T.; Qin, D.; Plattner, G.-K.; Tignor, M.; Allen, S.; Boschung, J.; Nauels, A.; Xia, Y.; Bex, V.; Midgley, P. (Eds.) Summary for Policymakers. In *Climate Change 2013: The Physical Science Basis. Contribution of Working Group I to the Fifth Assessment Report of the Intergovernmental Panel on Climate Change*; Cambridge University Press: Cambridge, UK; New York, NY, USA, 2014; p. 27.
2. Jena, P. Materials for Hydrogen Storage: Past, Present, and Future. *J. Phys. Chem. Lett.* **2011**, *2*, 206–211. [CrossRef]
3. Rivard, E.; Trudeau, M.; Zaghbi, K. Hydrogen Storage for Mobility: A Review. *Materials* **2019**, *12*, 1973. [CrossRef] [PubMed]
4. Sule, R.; Mishra, A.K.; Nkambule, T.T. Recent Advancement in Consolidation of MOFs as Absorbents for Hydrogen Storage. *Int. J. Energy Res.* **2021**, *45*, 12481–12499. [CrossRef]
5. DOE. Technical Targets for Onboard Hydrogen Storage for Light-Duty Vehicles. Available online: <https://www.energy.gov/eere/fuelcells/doe-technical-targets-onboard-hydrogen-storage-light-duty-vehicles> (accessed on 3 October 2022).
6. Murray, L.J.; Dincă, M.; Long, J.R. Hydrogen Storage in Metal–Organic Frameworks. *Chem. Soc. Rev.* **2009**, *38*, 1294–1314. [CrossRef] [PubMed]
7. Ren, J.; Langmi, H.W.; North, B.C.; Mathe, M. Review on Processing of Metal–Organic Framework (MOF) Materials towards System Integration for Hydrogen Storage. *Int. J. Energy Res.* **2015**, *39*, 607–620. [CrossRef]
8. Shet, S.P.; Shanmuga Priya, S.; Sudhakar, K.; Tahir, M. A Review on Current Trends in Potential Use of Metal–Organic Framework for Hydrogen Storage. *Int. J. Hydrogen Energy* **2021**, *46*, 11782–11803. [CrossRef]
9. Farha, O.K.; Yazaydin, A.Ö.; Eryazici, I.; Malliakas, C.D.; Hauser, B.G.; Kanatzidis, M.G.; Nguyen, S.T.; Snurr, R.Q.; Hupp, J.T. De Novo Synthesis of a Metal–Organic Framework Material Featuring Ultrahigh Surface Area and Gas Storage Capacities. *Nat. Chem.* **2010**, *2*, 944–948. [CrossRef]
10. Lochan, R.C.; Head-Gordon, M. Computational Studies of Molecular Hydrogen Binding Affinities: The Role of Dispersion Forces, Electrostatics, and Orbital Interactions. *Phys. Chem. Chem. Phys.* **2006**, *8*, 1357–1370. [CrossRef]
11. Kubo, M.; Ushiyama, H.; Shimojima, A.; Okubo, T. Investigation on Specific Adsorption of Hydrogen on Lithium-Doped Mesoporous Silica. *Adsorption* **2011**, *17*, 211–218. [CrossRef]
12. Han, S.S.; William, A.G., 3rd. Lithium-Doped Metal–Organic Frameworks for Reversible H<sub>2</sub> Storage at Ambient Temperature. *J. Am. Chem. Soc.* **2007**, *129*, 8422–8423. [CrossRef]
13. Xu, G.; Meng, Z.; Liu, Y.; Guo, X.; Deng, K.; Ding, L.; Lu, R. Porous MOF-205 with Multiple Modifications for Efficiently Storing Hydrogen and Methane as Well as Separating Carbon Dioxide from Hydrogen and Methane. *Int. J. Energy Res.* **2019**, *43*, 7517–7528. [CrossRef]
14. Himsl, D.; Wallacher, D.; Hartmann, M. Improving the Hydrogen-Adsorption Properties of a Hydroxy-Modified MIL-53(Al) Structural Analogue by Lithium Doping. *Angew. Chem. Int. Ed. Engl.* **2009**, *48*, 4639–4642. [CrossRef] [PubMed]
15. Kubo, M.; Shimojima, A.; Okubo, T. Effect of Lithium Doping into MIL-53(Al) through Thermal Decomposition of Anion Species on Hydrogen Adsorption. *J. Phys. Chem. C* **2012**, *116*, 10260–10265. [CrossRef]
16. Yang, S.; Lin, X.; Blake, A.J.; Walker, G.S.; Hubberstey, P.; Champness, N.R.; Schröder, M. Cation-Induced Kinetic Trapping and Enhanced Hydrogen Adsorption in a Modulated Anionic Metal–Organic Framework. *Nat. Chem.* **2009**, *1*, 487–493. [CrossRef] [PubMed]
17. Kubo, M.; Hagi, H.; Shimojima, A.; Okubo, T. Facile Synthesis of Hydroxy-Modified MOF-5 for Improving the Adsorption Capacity of Hydrogen by Lithium Doping. *Chem. Asian J.* **2013**, *8*, 2801–2806. [CrossRef]
18. Panchariya, D.K.; Kumar, E.A.; Singh, S.K. Lithium-Doped Silica-Rich MIL-101(Cr) for Enhanced Hydrogen Uptake. *Chem. Asian J.* **2019**, *14*, 3728–3735. [CrossRef]
19. Mulfort, K.L.; Farha, O.K.; Stern, C.L.; Sarjeant, A.A.; Hupp, J.T. Post-Synthesis Alkoxide Formation within Metal–Organic Framework Materials: A Strategy for Incorporating Highly Coordinatively Unsaturated Metal Ions. *J. Am. Chem. Soc.* **2009**, *131*, 3866–3868. [CrossRef]
20. Zhou, L.; Niu, Z.; Jin, X.; Tang, L.; Zhu, L. Effect of Lithium Doping on the Structures and CO<sub>2</sub> Adsorption Properties of Metal-organic Frameworks HKUST-1. *ChemistrySelect* **2018**, *3*, 12865–12870. [CrossRef]
21. Chuvikov, S.V.; Berdonosova, E.A.; Krautsou, A.; Kostina, J.V.; Minin, V.V.; Ugolokova, E.A.; Klyamkin, S.N. Peculiarities of High-Pressure Hydrogen Adsorption on Pt Catalyzed Cu-BTC Metal–Organic Framework. *Phys. Chem. Chem. Phys.* **2021**, *23*, 4277–4286. [CrossRef]
22. Zhang, W.; Kauer, M.; Halbherr, O.; Epp, K.; Guo, P.; Gonzalez, M.I.; Xiao, D.J.; Wiktor, C.; Lladrós I Xamena, F.X.; Wöll, C.; et al. Ruthenium Metal–Organic Frameworks with Different Defect Types: Influence on Porosity, Sorption, and Catalytic Properties. *Chemistry* **2016**, *22*, 14297–14307. [CrossRef]
23. Usman, M.; Iqbal, N.; Noor, T.; Zaman, N.; Asghar, A.; Abdelnaby, M.M.; Galadima, A.; Helal, A. Advanced Strategies in Metal–Organic Frameworks for CO<sub>2</sub> Capture and Separation. *Chem. Rec.* **2021**, *22*, e202100230. [CrossRef]

24. Iacomi, P.; Formalik, F.; Marreiros, J.; Shang, J.; Rogacka, J.; Mohmeyer, A.; Behrens, P.; Ameloot, R.; Kuchta, B.; Llewellyn, P.L. Role of Structural Defects in the Adsorption and Separation of C3 Hydrocarbons in Zr-Fumarate-MOF (MOF-801). *Chem. Mater.* **2019**, *31*, 8413–8423. [[CrossRef](#)]
25. Barin, G.; Krungleviciute, V.; Gutov, O.; Hupp, J.T.; Yildirim, T.; Farha, O.K. Defect Creation by Linker Fragmentation in Metal-Organic Frameworks and Its Effects on Gas Uptake Properties. *Inorg. Chem.* **2014**, *53*, 6914–6919. [[CrossRef](#)] [[PubMed](#)]
26. Chaemchuen, S.; Luo, Z.; Zhou, K.; Mousavi, B.; Phatanasri, S.; Jaroniec, M.; Verpoort, F. Defect Formation in Metal–Organic Frameworks Initiated by the Crystal Growth-Rate and Effect on Catalytic Performance. *J. Catal.* **2017**, *354*, 84–91. [[CrossRef](#)]
27. Kubo, M.; Saito, T.; Shimada, M. Evaluation of the Parameters Utilized for the Aerosol-Assisted Synthesis of HKUST-1. *Microporous Mesoporous Mater.* **2017**, *245*, 126–132. [[CrossRef](#)]
28. Kubo, M.; Sugahara, T.; Shimada, M. Facile Fabrication of HKUST-1 Thin Films and Free-Standing MWCNT/HKUST-1 Film Using a Spray-Assisted Method. *Microporous Mesoporous Mater.* **2021**, *312*, 110771. [[CrossRef](#)]
29. Kubo, M.; Ishimura, M.; Shimada, M. Improvement of Production Efficiency of Spray-Synthesized HKUST-1. *Adv. Powder Technol.* **2021**, *32*, 2370–2378. [[CrossRef](#)]
30. Kubo, M.; Moriyama, R.; Shimada, M. Facile Fabrication of HKUST-1 Nanocomposites Incorporating Fe<sub>3</sub>O<sub>4</sub> and TiO<sub>2</sub> Nanoparticles by a Spray-Assisted Synthetic Process and Their Dye Adsorption Performances. *Microporous Mesoporous Mater.* **2019**, *280*, 227–235. [[CrossRef](#)]
31. Kubo, M.; Matsumoto, T.; Shimada, M. Spray Synthesis of Pd Nanoparticle Incorporated HKUST-1, and Its Catalytic Activity for 4-Nitrophenol Reduction. *Adv. Powder Technol.* **2022**, *33*, 103701. [[CrossRef](#)]
32. Zhang, W.; Kauer, M.; Guo, P.; Kunze, S.; Cwik, S.; Muhler, M.; Wang, Y.; Epp, K.; Kieslich, G.; Fischer, R.A. Impact of Synthesis Parameters on the Formation of Defects in HKUST-1. *Eur. J. Inorg. Chem.* **2017**, *2017*, 925–931. [[CrossRef](#)]
33. Yang, S.; Lin, X.; Blake, A.J.; Thomas, K.M.; Hubberstey, P.; Champness, N.R.; Schröder, M. Enhancement of H<sub>2</sub> Adsorption in Li<sup>+</sup>-Exchanged Co-Ordination Framework Materials. *Chem. Commun.* **2008**, 6108–6110. [[CrossRef](#)] [[PubMed](#)]
34. Mulfort, K.L.; Wilson, T.M.; Wasielewski, M.R.; Hupp, J.T. Framework Reduction and Alkali-Metal Doping of a Triply Catenating Metal-Organic Framework Enhances and Then Diminishes H<sub>2</sub> Uptake. *Langmuir* **2009**, *25*, 503–508. [[CrossRef](#)] [[PubMed](#)]
35. Xiang, Z.; Hu, Z.; Yang, W.; Cao, D. Lithium Doping on Metal-Organic Frameworks for Enhancing H<sub>2</sub> Storage. *Int. J. Hydrogen Energy* **2012**, *37*, 946–950. [[CrossRef](#)]

**Disclaimer/Publisher’s Note:** The statements, opinions and data contained in all publications are solely those of the individual author(s) and contributor(s) and not of MDPI and/or the editor(s). MDPI and/or the editor(s) disclaim responsibility for any injury to people or property resulting from any ideas, methods, instructions or products referred to in the content.